4-20-2022

Study of Deexcitation Intensities to the K-Shell in Iron 55

Eric Helgemo
Western Michigan University, eric.s.helgemo@gmail.com

Study of Deexcitation Intensities to the K-Shell in Iron 55

Eric Helgemo

Lee Honors College

Western Michigan University

Department of Physics

Thesis Mentor: Dr. Michael Famiano

Thesis Committee:

Dr. Michael Famiano

Dr. Zbigniew Chajecki

Abstract

55Fe radioactive sources are used for x-ray calibration due to the long half-lives of 2.73 years and the optimal energies of the peaks. The source used in the experiment was generated using Western Michigan University's Tandem Van de Graff accelerator to produce a 6 MeV proton beam which induced a 55Mn(p, n)55Fe reaction on a 10 μm 55Mn target. The emissions from this target were then measured using a silicon lithium drift x-ray detector to determine the number of instances of deexcitation through kα and kβ modes. The preliminary data discussed showed a lower relative deexcitation rate of 6.67 between the kα and kβ x-ray emissions when compared to previous data indicating a ratio closer to 8.6, which is not accounted for in statistical error [1]. Future analysis will aim to explain this discrepancy, which is likely experimental as discussed in this paper. Should it be shown that the methods discussed in this paper are an effective means of decreasing error in measurements of these deexcitation intensities, it would have applications in x-ray telescope calibration. This would in turn reduce error in measurements taken by x-ray telescopes that utilize a 55Fe source for calibration.

Electron Capture and Deexcitation

Electron capture is a beta decay process where an electron from the k shell of an atom is absorbed into the nucleus, resulting in the conversion of a proton to a neutron. Decaying through this process results in a hole in the k shell as shown in image 1.

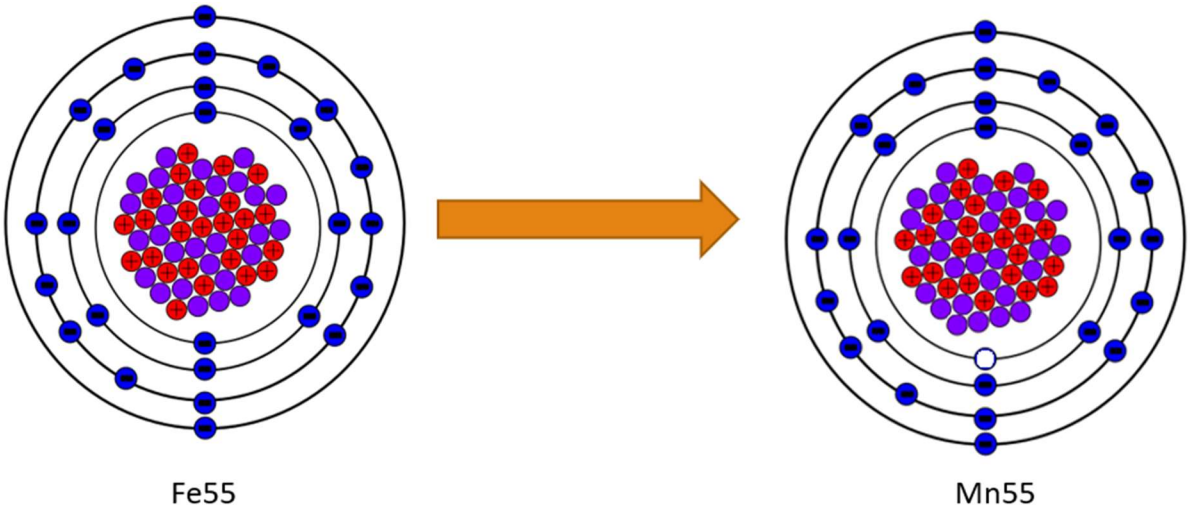

Image 1: This image shows the electron capture process of 55Fe + e → 55Mn. As a result of the nucleus absorbing an electron in the k shell, a hole is generated, which can be filled by deexcitation from upper shells.

The hole produced because of this process provides an opportunity for electrons from the M and L shells to deexcite. When electrons from the M shell deexcite to the K shell, the resulting characteristic x-ray is called a kα x-ray emission and likewise, an L shell deexcitation results in a kβ x-ray emission. The energies of these emissions are $k\alpha_1$ = 5.888 KeV, $k\alpha_2$ = 5.599 KeV, and kβ = 6.49 KeV for both $k\beta_1$ and $k\beta_2$ [1]. The minor differences in energy between the $k\alpha_1$ and $k\alpha_2$ emissions are due to the different spins of the electron that deexcites. The difference in energy of the $k\beta_1$ and $k\beta_2$ is lesser known but results from similarly spin related causes. The goal of this experiment was to measure the relative deexcitation rates of M and L

shell electrons to the K shell to demonstrate that improvements in the uncertainty of the known values were possible. The best-known values for these deexcitations can be found in the appendix in table 1 [1].

Tandem Van de Graff Accelerator Functions and Usage

The Western Michigan University (WMU) Tandem Van de Graff accelerator utilizes electrostatic potentials generated by 2 large Van de Graff generators [2]. This means that 2 metal belts are used to generate electrostatic potential across a large chamber. Protons are moved towards this chamber, where the fields generated due to the large electrostatic potential difference across the chamber induces acceleration of the beam down the beamline, generating packets of protons with energies upwards of 11 MeV. The packets of protons are then directed into a chamber where they can collide with a target material.

In this experiment, the Tandem Van de Graff accelerator was used to direct a 6 MeV beam of protons onto a 55Mn target, with the goal of inducing the 55Mn(p, n)55Fe nuclear reaction. The constraints for the beam line were found using the nuclear reaction equation 1 [3].

$$t = \frac{-1}{\lambda}\ln(1 - {}^{A}/_{\Phi N\sigma}) \quad (1)$$

In this equation, t is exposure time, $\lambda = {}^{\ln 2}/_{T_{1/2}}$, $T_{1/2}$ is the half-life of the material, A is the activity in becquerel, N is the number of target atoms per cm^2, σ is the nuclear reaction cross section, and Φ is the beam intensity. The nuclear reaction cross section for 55Mn(p, n)55Fe was found using the JANIS database with TENDEL simulated incident proton data [4-5].

Silicon Lithium Drift X-Ray Detector

The x-ray detector used in the experiment was a silicon lithium drift (SiLi) x-ray detector [6]. This was because the range of operation was optimal, allowing for most of the x-rays released by the 55Fe source to be captured. The operational range is shown in image 2.

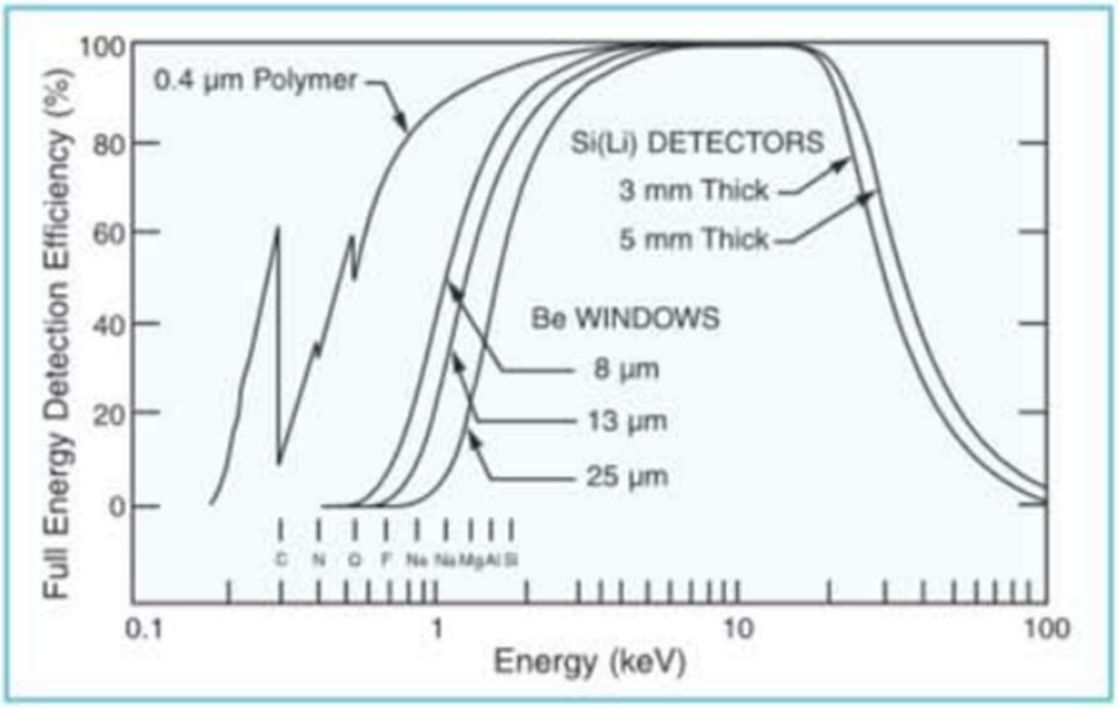

Image 2: This is the efficiency curve for the SiLi detector used in the experiment. This detector has an efficiency of 96% to 100% over the interval of interest.

This detector did not have large enough channel width to distinguish between either $k\alpha_1$ and $k\alpha_2$ or $k\beta_1$ and $k\beta_2$, as it was found to have a channel width of approximately 22 eV. For this reason, all preliminary data is discussed in terms of the kα and kβ peaks. Once the data was collected from the SiLi detector, a python program was written to analyze the ascii data sheets and produce fits of the data to gaussians to check for normalcy in the data.

Applications

This research aims to demonstrate that an improvement in the measurement error of the deexcitation intensities of a 55Fe sample can be achieved with the proper methodology and equipment. The reduced error in these results would allow for improved calibration of x-ray observatories and telescopes on Earth and in space. X-ray telescopes in space take x-ray sources with them to routinely recalibrate their detectors. One such common source for calibrations of this type is 55Fe. By reducing the error in the known values for the deexcitation intensities of kα and kβ emissions emitted from the 55Fe source, the telescopes that calibrate using this will see a similar decrease in the systematic error that must be accounted for when calculating error in any measurement taken. With a reduction from 10% error down to 1% error in deexcitation intensity values, modern measurement methods would allow us to address several important scientific questions that include improved measurements of the Hubble constant [7-10], determination of cosmological constrains from galactic clusters, the study of the cosmic X-ray background [11], and exploration of the nature of black holes and neutron stars [12].

Preliminary Results

The x-ray spectrum generated by the 55Fe sources is shown in graph 1 and 2. Graph 1 shows the energy in KeV vs the Counts on a linear scale, where there is a minimal effect on the data due to the background radiation. In graph 2, the same data is shown where the axis are energy in KeV vs $\log_{10}$(counts). This allows for the identification of 3 peaks in the region of interest.

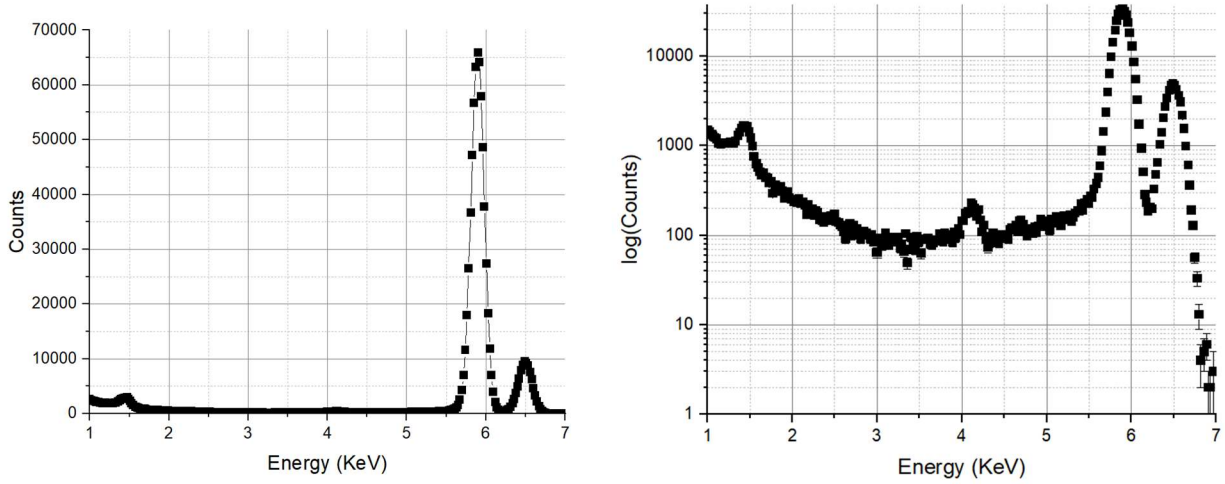

Graph 1 and 2: In graph 1 on the left, the scales are linear showing that the background is largely insignificant in the data relative to the kα and kβ peaks. In graph 2 on the right, the log of the counts is shown. This shows that there are 3 peaks in the data.

These peaks are fitted to a gaussian in graphs 3, 4, and 5. Graph 3 shows a gauss fit of the kα peak. This graph fits the gaussian, indicating that there is not a significant smaller peak from a different material effecting this data.

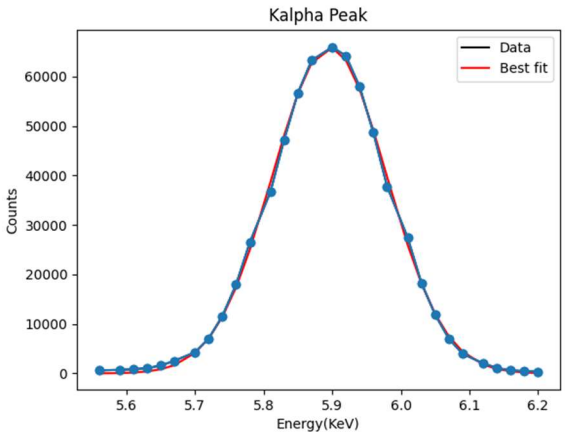

Graph 3: This graph shows a gaussian fit of the data for the kα peak, indicating that the curve is gaussian.

In graph 4, the kβ peak was fitted with a gaussian. The graph fits well apart from the raised lower energy end of the curve. This indicates that there is some overlap of the data from the kα with the kβ curve. Aside from this overlap, the curve fits a gaussian, suggesting there is also not a significant smaller peak from a different decay process contained in the peak.

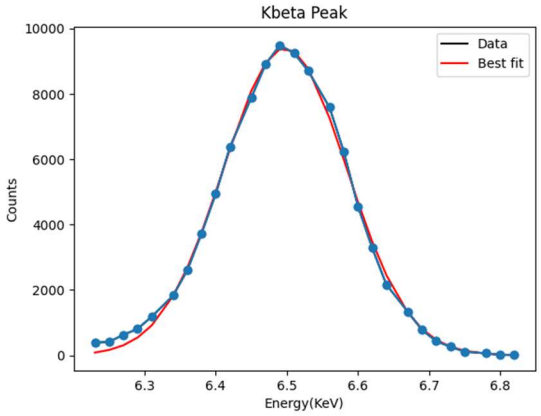

Graph 4: This graph shows a gaussian fit of the data for the kβ peak, indicating that the curve is gaussian. The lower energy is offset from the gaussian, indicating an overlap with the kα peak.

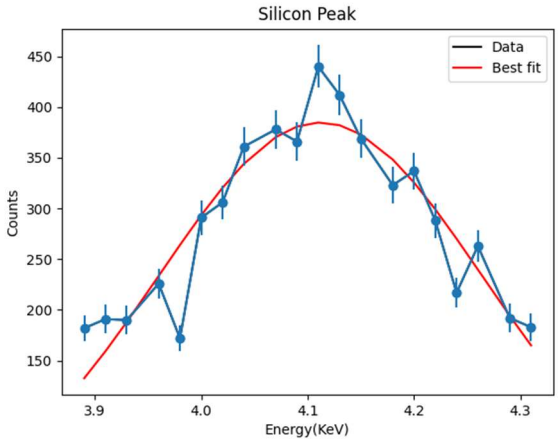

Graph 5: This graph shows the silicon escape peak that is seen in graph 2.

In graph 5, the lowest energy peak is found to be a silicon escape peak. This is generated from partially irradiated sections of the SiLi detector. Due to the lower counts creating high statistical error, it does not quite fit a gaussian. The low counts and peak energy difference between the escape peak and the kα peak indicates that this does not have a significant effect on the data.

Analysis and Discussion

The upper bound on the experimental error in the relative deexcitation of the kα and kβ peaks from previous data can be found to be around 8.6 ± 0.8 [1]. When dividing the total counts under the kα and kβ curves, a ratio of 6.67 ± 0.02 is found. The error in this is purely statistical, so the experimental error has not been accounted for in this data. Unless there is an extreme source of error in this data, the values can not be within error of one another. This indicates that there is either an issue in the experimental setup or in the methodology.

The first aspect to check for the source of this error is if there are any elements that have extremely similar peak energies that could fit the data effectively enough to not be detected through gaussian analysis. The only candidate for this is 55Co, which can be generated in this system via a secondary (p, n) process. While the original process used to generate the 55Fe source was 55Mn(p, n)55Fe, a secondary process is 55Fe(p, n)55Co. This can be ruled out due to the half life of 55Co. Since 55Co has a half-life of 17.5 hours, if this was the source of the discrepancy, then this discrepancy would decrease over the time of the data collection. In this experiment, 5 ascii sheets were generated by the SiLi detector due to brief periods where the detector was shut off to refill with liquid nitrogen. Graph 6 was generated by looking at the

combined data with statistical error in these results. Given the large exposure time, if this result was due to 55Co, the graph would show the ratio increasing as the 55Co decayed.

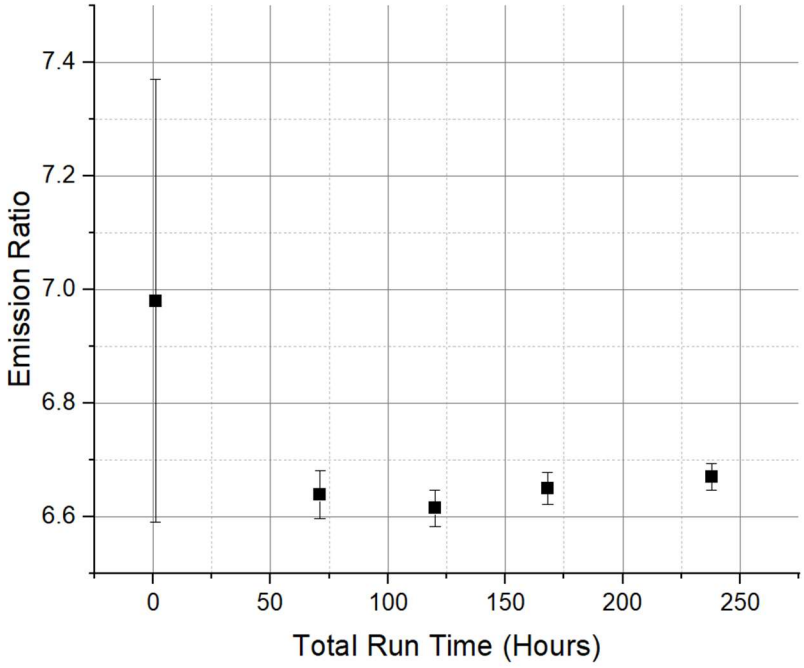

Graph 6: In this graph, the emission ratios for the 5 data sheets were analyzed, showing that the emission ratio was consistent within error through the whole experiment. This indicates that the discrepancy was not due to a short-lived radioactive nucleus under the kβ curve.

The efficiency of the detector is also not the source of the error. For this error to be due to detector efficiency, it would require an efficiency difference at the peaks of the 2 curves to be 15%. However, since the efficiency is between 96% and 100% over the interval of interest, this is not the source. This can also not be due to the cosmic ray background, as the background seen in graphs 1 and 2 is too small to have an effect this large in the data set. Future analysis of the experimental setup will seek to determine the source of the error in this data and use a higher activity target to obtain more substantive data.

References

[1] Junde, H. (2008). Nuclear data sheets for a = 55. *Nuclear Data Sheets*, *109*(4), 787-942. https://doi.org/10.1016/j.nds.2008.03.001

[2] Ferguson, S.M., & Parpart, L.R. (1982). Western Michigan University 1982 SNEAP Laboratory report (DOE/ER/40048--24-L2). United States

[3] Martin, B. R., & Shaw, G. (2019). Nuclear and particle physics: An introduction.

[4] N. Soppera, M. Bossant, E. Dupont, "JANIS 4: An Improved Version of the NEA Java-based Nuclear Data Information System", Nuclear Data Sheets, Volume 120, June 2014

[5] D. Rochman, A.J. Koning, J.Ch. Sublet, M. Fleming, et al, "The TENDL library: hope, reality and future", proceedings of the International Conference on Nuclear Data for Science and Technology, September 11-16, 2016, Bruges, Belgium

[6] *SiLi Detectors for X-Ray Spectroscopy*. (2017). Retrieved 12 December 2021, from http://www.canberra.com

[7] J. Silk and S. D. M. White. The determination of q0 using X-ray and microwave observation of galaxy clusters. , 226:L103–L106, December 1978.

[8] M. Birkinshaw. Limits to the value of the Hubble constant deduced from observations of clusters of galaxies, 187:847–862, June 1979.

[9] Roberto Scaramella, Renyue Cen, and Jeremiah P. Ostriker. A Hydrodynamic Approach to Cosmology: Nonlinear Effects on Cosmic Backgrounds in the Cold Dark Matter Model. , 416:399, October 1993.

[10] A. Cavaliere, L. Danese, and G. de Zotti. Unborn clusters, 217:6–15, October 1977.

[11] Bobin, J., Sureau, F., & Starck, J. (2016). Cosmic microwave background reconstruction from WMAP, Planck, PR2 data. *Astronomy &Amp; Astrophysics*, *591*, A50. https://doi.org/10.1051/0004-6361/201527822

[12] Feryal Özel *et al* 2016 *ApJ* 832 92

Appendix

Transition Type	Intensity	Error
$k\alpha_1$	16.2% ± 0.7	± 4.3%
$K\alpha_2$	8.2% ± 0.4	± 4.9%
$k\beta_1$	1.89% ± 0.09	± 4.8%
$K\beta_2$	0.96% ± 0.05	± 5.2%

Table 1: These are the best known deexcitation intensities for 55Mn. The table shows that there is an uncertainty in these measurements of around 10%, which contributes to uncertainty when used for calibrations. The remaining intensity is found in processes that weren't observed in the experiment as well as in the Bremsstrahlung radiation generated from the Auger electrons generated during 55Fe decay.